Microfluidic evidence of synergistic effects between mesenchymal stromal cell-derived biochemical factors and biomechanical forces to control endothelial cell function

Zhang, Shuang; Tuk, Bastiaan; van de Peppel, Jeroen; Kremers, Gert Jan; Koedam, Marijke; Pesch, Georg R.; Rahman, Zaid; Hoogenboezem, Remco M.; Boukany, Pouyan E.; More Authors

DOI
10.1016/j.actbio.2022.08.025

Publication date
2022

Document Version
Final published version

Published in
Acta Biomaterialia

Acta Biomaterialia 151 (2022) 346–359

Contents lists available at ScienceDirect

Acta Biomaterialia

journal homepage: www.elsevier.com/locate/actbio

Full length article

Microfluidic evidence of synergistic effects between mesenchymal stromal cell-derived biochemical factors and biomechanical forces to control endothelial cell function

Shuang Zhang[a], Bastiaan Tuk[b], Jeroen van de Peppel[a], Gert-Jan Kremers[c], Marijke Koedam[a], Georg R. Pesch[d], Zaid Rahman[d], Remco M. Hoogenboezem[e], Eric M.J. Bindels[e], Johan W. van Neck[b], Pouyan E. Boukany[d], Johannes P.T.M. van Leeuwen[a], Bram C.J. van der Eerden[a,*]

[a] Laboratory for Calcium and Bone Metabolism, Department of Internal Medicine, Erasmus University Medical Center; Rotterdam, the Netherlands
[b] Department of Plastic and Reconstructive Surgery, Erasmus University Medical Center; Rotterdam, the Netherlands
[c] Erasmus Optical Imaging Center, Erasmus University Medical Center; Rotterdam, the Netherlands
[d] Department of Chemical Engineering, Delft University of Technology; Delft, the Netherlands
[e] Department of Hematology, Erasmus University Medical Center; Rotterdam, the Netherlands

ARTICLE INFO

Article history:
Received 28 March 2022
Revised 20 July 2022
Accepted 12 August 2022
Available online 20 August 2022

Keywords:
Microfluidics
Endothelial cell
Mesenchymal stromal cell
Angiogenesis

ABSTRACT

A functional vascular system is a prerequisite for bone repair as disturbed angiogenesis often causes non-union. Paracrine factors released from human bone marrow derived mesenchymal stromal cells (BMSCs) have angiogenic effects on endothelial cells. However, whether these paracrine factors participate in blood flow dynamics within bone capillaries remains poorly understood. Here, we used two different microfluidic designs to investigate critical steps during angiogenesis and found pronounced effects of endothelial cell proliferation as well as chemotactic and mechanotactic migration induced by BMSC conditioned medium (CM). The application of BMSC-CM in dynamic cultures demonstrates that bioactive factors in combination with fluidic flow-induced biomechanical signals significantly enhanced endothelial cell migration. Transcriptional analyses of endothelial cells demonstrate the induction of a unique gene expression profile related to tricarboxylic acid cycle and energy metabolism by the combination of BMSC-CM factors and shear stress, which opens an interesting avenue to explore during fracture healing. Our results stress the importance of *in vivo* - like microenvironments simultaneously including biochemical, biomechanical and oxygen levels when investigating key events during vessel repair.

Statement of significance

Our results demonstrate the importance of recapitulating *in vivo* - like microenvironments when investigating key events during vessel repair. Endothelial cells exhibit enhanced angiogenesis characteristics when simultaneous exposing them to hMSC-CM, mechanical forces and biochemical signals simultaneously. The improved angiogenesis may not only result from the direct effect of growth factors, but also by reprogramming of endothelial cell metabolism. Moreover, with this model we demonstrated a synergistic impact of mechanical forces and biochemical factors on endothelial cell behavior and the expression of genes involved in the TCA cycle and energy metabolism, which opens an interesting new avenue to stimulate angiogenesis during fracture healing.

1. Introduction

Fracture repair is a unique process that can restore original geometry and biomechanical properties of the injured bone without the formation of scar tissue through a regenerative process in a well-orchestrated way [1]. However, a significant proportion of

* Corresponding author.
E-mail address: b.vandereerden@erasmusmc.nl (B.C.J. van der Eerden).

https://doi.org/10.1016/j.actbio.2022.08.025
1742-7061/

clinical scenarios still display compromised regeneration, resulting in delayed union and complications including non-union. Incidence of reported non-union fracture remains variable, depending on patient demographics, standard criteria, anatomic regions, but ranges from anywhere between 1.9 and 4.9 % [2,3], with an estimated 100,000 cases of non-union per year in the United States alone [4].

Risks of non-union can be considered as both patient-dependent and -independent. Patient-dependent risk factors, such as smoking and diabetes mellitus cause delayed chondrogenesis and soft callus formation through arteriolar blood flow damage [5,6]. The method of fracture fixation as a patient-independent risk also alters blood supply at the skeletal healing site. Intramedullary nails can impede endosteal circulation [7], independent of whether nail insertion was performed with or without reaming of the medullary cavity [8]. Furthermore, long-standing clinical evidence has shown a strong correlation between angiogenesis and fracture healing, indicating the importance of vessel restoration process [9,10].

The process of fracture healing can be divided into three biological phases: inflammation, repair and remodeling. The inflammatory response is initiated by tissue damage and characterized by hematoma formation, together with the release of inflammatory cytokines and angiogenic factors as a result of the hypoxic conditions created by the vascular disruption [11]. The repair phase begins with callus formation allowing blood vessels to invade the calcified tissue and coordinate with osteoblasts to build new bone [12]. Therefore, this neovascularization is required for osteoprogenitors recruitment and crucial to re-establish oxygenation [13,14]. In contrast to hypervascularization of the fracture site during the repair phase, vascularization is reduced to pre-injury level in the remodeling phase [15]. Moreover, studies have demonstrated that fracture healing is completely inhibited after treatment with an angiogenesis inhibitor [16]. Therefore, adequate blood supply is a prerequisite for bone repair at the fracture site.

Human mesenchymal stromal cells (MSCs) are highly angiogenic and have the potential to promote bone vascularization via at least two distinct mechanisms; 1) by paracrine effects, which include cytokines release and exosomes transfer [17,18], or 2) by direct differentiation into vascular–like cells to subsequently promote angiogenesis [19]. Accumulating data has shown that the therapeutic effect of MSCs was mediated primarily by paracrine factors rather than their differentiation potential, as the engrafted cells were hardly found 4 weeks after transplantation *in vivo* [19]. Moreover, the bioactive factors released from MSCs can bypass the present confounding issues of MSC themselves related to cell transplantation, manufacturing and costs, providing the possibility to be used extensively [20]. Furthermore, it should be realized that several bioactive factors in the MSC secretome promote angiogenesis in a well-coordinated way [21], and this effect is synergistic compared to the administration of single factors, which are insufficient to stimulate angiogenesis due to low efficacy [22].

Several *in vitro* models have been developed that show the beneficial effect of MSC-secretome on angiogenesis [23,24]. However, the intricate microenvironment of vessel repair is composed of numerous components, such as mechanical forces (fluid flow), hypoxia, and biological factors, which regulate critical steps of the recovery process in a coordinated fashion. To date, no suitable model has been fully recapitulating the vessel repair environment by simultaneously evaluating the contribution of biological factors and mechanical forces or even their combination to angiogenesis. Deeper insight into the effect of the MSC-secretome on angiogenesis strongly depends on the progression towards better models emulating the physiological and pathological microenvironment *in vivo*. In this study, we developed an *in vivo* - like microenvironment model that enables manipulating the mentioned extrinsic factors and we applied this model to study the MSC - endothelial cell interaction. The resulting microfluidic designs better elucidate complex relationship between biological and mechanical signals in a hypoxia microenvironment and provide insights into energy metabolism-triggered angiogenesis.

2. Materials and methods

2.1. Cell culture

Human bone marrow derived mesenchymal stromal cells (BMSCs, Lonza, Basel, Switzerland) were cultured as described previously [25]. Briefly, BMSCs were cultured in alpha minimum essential medium (α-MEM, Gibco, Paisley, UK) supplemented with 10% heat-inactivated fetal calf serum (FCS). Cells at passage 7 were used to prepare conditioned medium. Human umbilical vein endothelial cells (HUVECs, Lonza, Basel, Switzerland) were maintained in Endothelial Growth Medium (EGM-2, Lonza, Basel, Switzerland) and cells up to passage 6 were used for the experiments. Human Aortic Endothelial Cells (HAECs, PromoCell, Huissen, The Netherlands) were cultured in Endothelial Cell Growth Medium MV (PromoCell, Huissen, The Netherlands). Cells at passage 4 were used for the experiments. All BMSCs and endothelial cells were maintained at 37°C containing 5% CO_2 in a humidified atmosphere.

2.2. Preparation of conditioned medium from BMSCs

BMSCs were seeded into T75 cm^2 flasks at a density of 10^4 cells/cm^2 and grown until 70-80% confluence. After washes, cells were refreshed with α-MEM containing 0.1% BSA, and incubated under 3% O_2 for 48h as described [26]. Supernatant (conditioned medium) was collected and centrifuged at 1,500 rpm for 5 min, filtered through a 0.22 µm filters and then stored in aliquots at -80°C as BMSC-CM.

A dilution of 50% *v*/v BMSC-CM in either Endothelial Basal Medium (EBM-2) or EGM-2 was used to evaluate its angiogenic properties. 50% *v*/v of α-MEM containing 0.1% BSA in EBM-2 or EGM-2 served as control (Ctrl). FCS concentration was maintained as 2% in each experimental group. We used cobalt(II) chloride ($CoCl_2$; Sigma-Aldrich, St. Louis, MO, USA) at a concentration of 300 µM to mimic the hypoxia effect in all experiments except the adhesion assay, considering the short treatment time in this experiment [27].

2.3. Angiogenic protein profile of BMSC-CM

BMSC-CM-derived angiogenesis-related proteins were screened using a Human Angiogenesis Antibody Array kit (Proteome profiler™; R&D Systems, Minneapolis, MN, USA). Briefly, BMSC-CM was mixed with a biotinylated antibody cocktail and then incubated with capture antibodies, which have been spotted onto nitrocellulose membranes in duplicate. Streptavidin–HRP and chemiluminescent detection reagents were used for visualization and development. The band densities were analyzed with Gel Doc XR System (Bio-Rad Laboratories, CA, USA). Positive signals on the developed membranes were quantified using the Fiji image processing program (NIH, Bethesda, MD, USA; https://imagej.net/Fiji) [28]. For quantification, each angiogenesis-related protein was determined by averaging the signal of duplicate spots, followed by subtraction of the background signal. Functional annotation of angiogenesis gene interaction was performed using GeneMANIA (http://www.genemania.org/) [29].

2.4. Cell morphology and adhesion assay

HUVECs were seeded in 96-well plate at a density of 2×10^5 cells/ml and allowed to attach for 15, 30, 45 and 60 min at 37°C.

Non-adherent cells were washed out by PBS, whereas adherent cells were fixed with 4% paraformaldehyde (PFA) and stained with 0.3% crystal violet. Cell morphology was examined on a Zeiss Axiovert 200 MOT microscope (Zeiss, Oberkochen, Germany). Cell number and cell surface area were quantified using Fiji software.

2.5. Wound healing assay and cell proliferation assay

Wound healing assays and Ki67 immunostaining were performed to determine migration and proliferation abilities of endothelial cells treated with BMSC-CM, respectively. For wound healing experiments, 4×10^4 HUVECs were seeded in each well of a 48-well plate. On the next day, the confluent cell layer was scratched with a 1 ml pipette tip, followed by 3 PBS washes. Cell migration was evaluated by measuring the width of the wound at 0, 8, 24 and 32 h post-scratching using Fiji software. For proliferation assay, HUVECs or HAECs were fixed with 4% PFA after 24 h and stained with ki67 antibody (1:100, Novus biological, Colorado, USA).

2.6. Gene expression analysis

RNA isolation, cDNA synthesis and real-time PCR reactions were performed as described before [25]. Oligonucleotide primer pairs were designed to be either on exon boundaries or spanning at least one intron (Table S1). Gene expression was normalized to the housekeeping gene *36B4*, using the equation $2^{\wedge\text{-}(\text{Ct gene of interest} - \text{Ct housekeeping gene})}$.

2.7. RNA-sequencing

Total RNA was isolated from 12-well plates using TRIzol (Thermo Fisher Scientific, Massachusetts, USA) as previously described [25,30]. To isolate RNA from microfluidic device, TRIzol was used to flush through the channel after PBS washes, followed by several times pipetting to thoroughly lyse all cells. RNA concentration and size distribution profiles were analyzed on an Agilent Bioanalyzer RNA 6000 Pico chip (Thermo Fisher Scientific, Massachusetts, USA). cDNA library was prepared using SMARTer version v4 Ultra Low Input RNA kit (Clontech, Takara Bio, California, USA). The resulting bulk RNA-seq libraries were generated with the Truseq nano DNA sample prep kit (Illumina, California, USA) based on the manufacturer's manual. The subsequent libraries were quality-checked and sequenced paired-end for 100 cycles on a Novaseq6000 instrument (Illumina, California, USA). Gene expression values were measured as Transcripts Per Kilobase (TPM). After mapping the reads, differential expression analysis was performed using the DESeq2 package in R environment [31]. Genes with an adjusted p-value < 0.05 and a $\log_2$-fold change ≥ 1 were considered significant.

Gene ontology (GO) analyses were performed using R packages [32], and GO terms were trimmed and summarized using REVIGO (http://revigo.irb.hr) [33]. Gene set enrichment analysis (GSEA) was performed on the normalized TPM values using gene sets with MSigDB [34].

2.8. Microfluidic device fabrication

Microfluidic chips were fabricated using standard soft lithography techniques [35]. The required master mold was fabricated using photolithography with SU-8 on a silicon wafer (Fig. S1A). A vector graphic of the microchannels was created using AutoCAD (Autodesk) and the photo masks were produced by CAD/Art Services Inc. with a resolution of 20,000 dpi. The dimensions of the microchannels used to evaluate cell proliferation (design 1) were 2 cm × 1 mm × 0.1 mm (length × width × height). For cell migration assays (design 2), the dimensions of the channels were 1.5 cm × 1 mm × 0.1 mm (length × width × height) separated by three short inlet channels on both ends. The channels were generated by casting polydimethylsiloxane (PDMS) at a 10:1 ratio of base to curing agent (Sylgard 184, Mavom, The Netherlands) on the master mold. PDMS was degassed until all bubbles were removed and cured at 70°C for at least 4 h. After crosslinking, PDMS was removed from the mold and bound to a glass coverslip using plasma treatment for 2 minutes and 20 seconds at 4 mbar pressure (Fig. S1A).

2.9. Microfluidic cell seeding, staining and viability

The microchannels were coated with 40 µg/ml fibronectin (Sigma-Aldrich, St. Louis, MO, USA) and kept in a humidified incubator overnight before seeding cells into the microfluidic device. To visualize the endothelial cells in the microchannel, HUVECs were stained with 4.5 µM CellTracker™ Green CMFDA (Life Technology, Carlsbad, CA, USA) at 37°C for 40 min using the recommended protocol.

A live/dead fluorescence labelling was used to determine the viability of the HUVECs. As previously described [36], cells were incubated in a mixture of 5 µg/mL Hoechst 33342 (Sigma-Aldrich, St. Louis, MO, USA) and 10 mg/mL propidium iodide (Sigma-Aldrich, St. Louis, MO, USA) for 15 min at 37°C. In this fluorescence-based assay, all cells were stained with Hoechst (blue), while only dead cells were labeled by propidium iodide (red).

All the fluorescent images and overlapping tiled images of the microfluidic devices were acquired on a Leica TCS SP5 confocal laser scanning microscope (Leica Microsystems, Mannheim, Germany).

2.10. Proliferation assay and flow experiments in the microfluidic single channel device (design 1)

HUVECs or HAECs were seeded on the fibronectin-coated microchannel at a density of 3×10^6 cells/ml and exposed to a flow rate at 0.5 µl/min after overnight attachment. Cell proliferation was evaluated by ki67 immunostaining staining after 24h. To evaluate potential morphological changes induced by BMSC-CM, cells were seeded in the single channel microfluidic device at a density of 7×10^6 cells/ml for 24h to attain a confluent monolayer with tight cell-cell contacts. Microfluidic chips were then connected to the syringe pump (New Era Pump Systems Inc, Farmingdale, NY, USA) and the flow rate was set at 3 µl/min.

2.11. Wound preparation, gradient characterization and migration in the microfluidic-based migration model (design 2)

HUVECs were seeded in the microfluidic device at a density of 5×10^6 cells/ml, and the wound was prepared by introducing parallel laminar flows into the channel from three separate inlets, which are each connected to their own syringe via polytetrafluoroethylene tubing (Diba Ltd. Cambridge, UK). The syringes on both sides contained EBM-2 supplemented with 2% FCS, while the syringe for the middle laminar flow contained trypsin-EDTA, all flowing into the microchannel at a rate of 80 µl/min for 5 min. After this, the channels were flushed with EGM-2 to remove floating cells, and cell migration towards the middle under different conditions were then observed.

To estimate the shape of growth factors gradient, 10-kDa FITC-dextran and 40-kDa FITC dextran (125 µg/ml for both dextrans, Sigma-Aldrich, St. Louis, MO, USA) were infused in the middle syringe to represent diffusion of angiogenic factors with different sizes, while PBS was infused in both side syringes. To mimic

chemotactic response induced by BMSC-CM, the contents in the syringes on both sides were replaced with EBM-2 containing 2% FCS, and the content in the middle syringe was replaced with control medium or BMSC-CM.

To evaluate the response of angiogenic factors on shear stress-induced HUVEC migration, control medium or BMSC-CM was introduced into all three syringes. HUVECs seeded in the microfluidic devices without the pump connection were considered as static culture.

The total flow rate through the channel connected with three inlets was set to 3 μl/min. Pictures were taken in the center of the microchannel at 0 and 6 hour, and wound area was measured by Fiji image analysis software.

2.12. Time-lapse microscopy

Time-lapse imaging was carried out on a Leica TCS SP5 confocal laser scanning microscope (Leica Microsystems, Mannheim, Germany) with a motorized stages enclosed in a humidified chamber at 37°C. Three fields of view were captured from each channel using a 5 × objective at 10 min intervals. Trajectories of 35-40 cells in the field of each image sequence were manually tracked using a Fiji Manual Tracking plugin. The chemotactic effect and was evaluated using Ibidi Chemotaxis and Migration Tool based on the manufacturer's instruction [37].

2.13. Fluorescence immunostaining staining

Immunostaining was performed as previously described [30]. Briefly, HUVECs were fixed with 4% PFA in PBS for 5 min and then washed with PBS. Immunostaining was performed after permeabilization in PBS with 0.1% Triton X-100 (Sigma-Aldrich, St. Louis, MO, USA) and blocking for 30 min in 1% bovine serum albumin at room temperature (RT). Cells were incubated with CD31 antibody (1:100, Abcam, Cambridge, UK), Ki67 antibody (1:100, Novus biological, Colorado, USA) or VE-Cadherin antibody (1:100, R&D systems, Minneapolis, MN, USA) overnight at 4°C. The next day, cells were incubated with Alexa Flour 488 donkey anti-mouse (1:300, Abcam, Cambridge, UK), or donkey anti-rabbit (1:300, Abcam, Cambridge, UK) secondary antibody for 1 hour at RT, followed by the addition of rhodamine-conjugated phalloidin (1:100, Thermo Fisher Scientific, Massachusetts, USA) for 1 hour at RT. After 10 min incubation with DAPI, images were captured on a Leica TCS SP5 confocal laser scanning microscope. Quantitative morphometric analyses were performed using image analysis software Fiji. The Ki67 index was used to evaluate ki67 proliferation. Calculation of the Ki67 index = No. of positive staining cells / total No. of cells × 100.

2.14. Statistical analysis

Data were expressed as means ± SEM of representative experiments. All experiments were performed at least 2 times. Statistical analysis was performed using GraphPad Prism 9. Significance was calculated using the Student's *t*-test or one-way ANOVA. Two-way ANOVA analysis was used to assess interaction between treatments. *P* values were considered significant if $p < 0.05$.

2.15. Data availability

The data that support the findings of this study are available within this paper, supplementary information or from the corresponding author upon reasonable request. All of the RNA-seq data that support the findings of this study have been deposited in Gene Expression Omnibus (GEO) with the accession number GSE208335. Source data are provided with this paper.

3. Results

3.1. Characterization of BMSC-derived conditioned medium

An overview of our experimental approach is depicted in Fig. 1. Endothelial cell behavior towards BMSC-CM was evaluated in static cell cultures and microfluidic models, followed by RNA-seq analyses in both conditions.

As shown in Fig. 2A, BMSCs were cultured 2 days under hypoxia with serum deprivation medium after initial expansion. To determine the presence of angiogenesis-related proteins in BMSC-CM, a membrane-based sandwich immunoassay was used. A broad spectrum of proangiogenic factors such as vascular endothelial cell growth factor (VEGF), monocyte chemotactic protein-1 (MCP-1) and angiogenin were secreted in BMSC-CM (Fig. 2B-C). In addition, some endogenous angiogenesis inhibitors such as thrombospondin-1 (TSP1), urokinase plasminogen activator (uPA), and plasminogen activator inhibitor (PAI-1)/serpin E1 were also detected in BMSC-CM (Fig. 2B-C). The protein association network constructed using GeneMANIA revealed a high interconnectivity between these proteins responsible for various angiogenesis functions but also with many other related proteins (Fig. 2D).

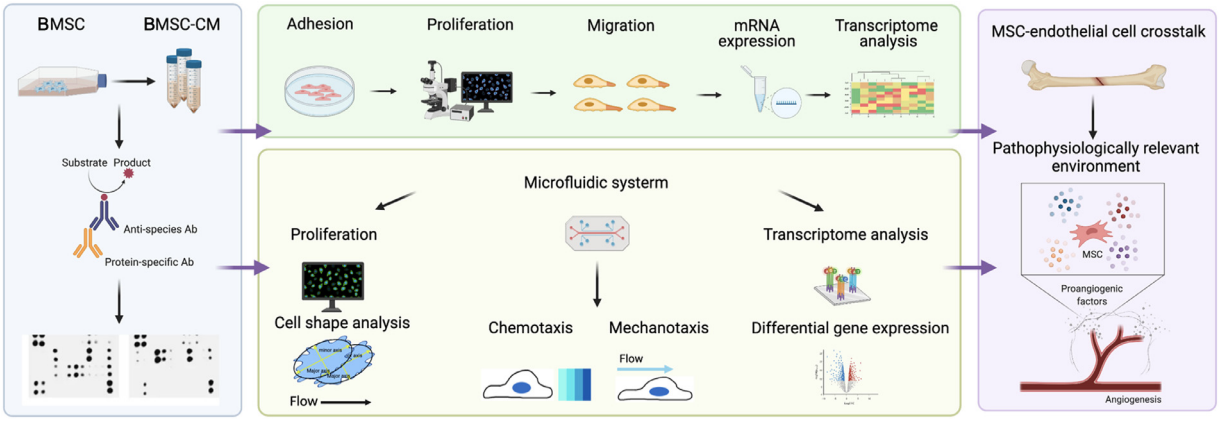

Fig. 1. Study design. A schematic overview of the experimental design and RNA-seq analysis. Our approach incorporated static cell culture and microfluidic cell culture models under a pathophysiological microenvironment including vessel damage, continues flow, hypoxia, and biological factors, and gene expression signatures assessed by transcriptome profiling.

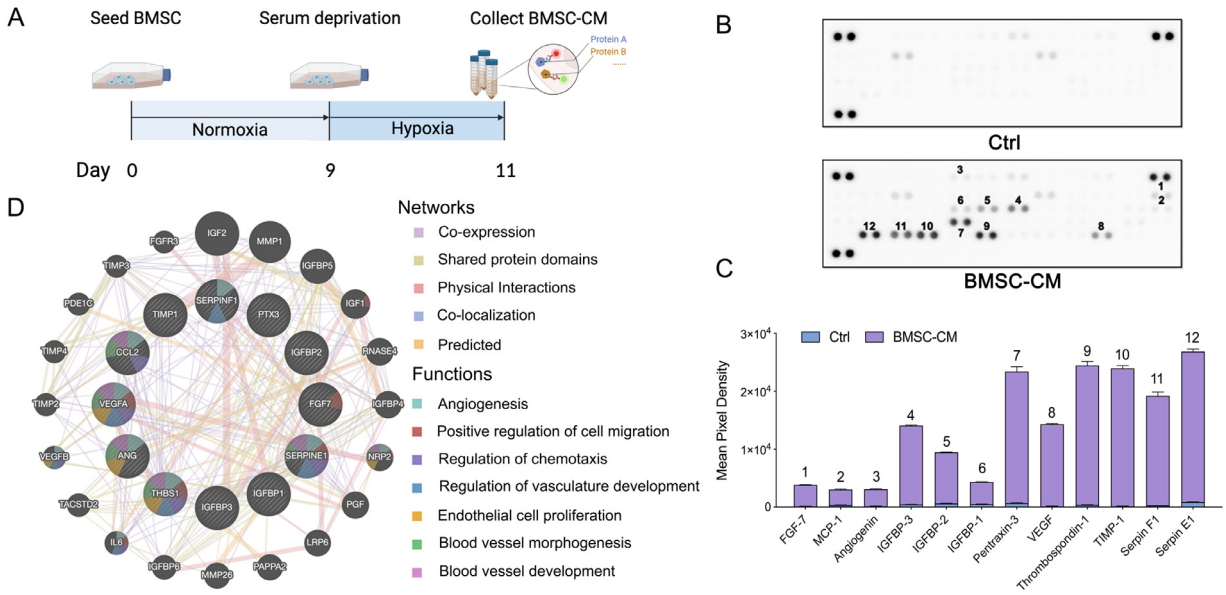

Fig. 2. Angiogenic protein profile of BMSC-CM. A Schematic diagram of BMSC-CM collection. **B-C** Angiogenesis-related proteins in BMSC-CM detected by human angiogenesis antibody array. α-MEM containing 0.1% BSA served as control. Quantification of mean spot pixel density using Fiji, and grey values were normalized to reference spots represented in top left, top right, and bottom left on the membranes. Target proteins are indicated 1-12 on the array membrane (**B**) and histogram (**C**). **D** Network analyses of 12 proteins according to different interaction categories and protein functions based on GeneMANIA analysis using an automatically selected weighting method. The inner circle nodes indicate the query genes, while the outer circle nodes were those selected by GeneMANIA. The size of the nodes in the outer circle indicates the relatedness to the query gene list.

3.2. BMSC-CM stimulates endothelial cell function

Several critical steps such as cell adhesion, proliferation and migration contribute to angiogenesis and vessel development. To mimic a stable hypoxia *in vivo* - like environment caused by vessel disruption, endothelial cells were cultured in $CoCl_2$-supplemented medium.

We first investigated the effect of BMSC-CM on HUVEC cell attachment and morphology. As shown by crystal violet staining, the number of adhered cells and total cell area were significantly higher in conditioned medium group at all investigated time points in both EBM-2 and EGM-2 condition (Fig. S2A-C and Fig. S4A-C). Cell proliferation was evaluated by cell number measurement and Ki67 immunostaining and bothwere significantly upregulated (1.5-fold) in response to BMSC-CM after 24 hours (Fig. S2D-F), which was supported by the observations on HAECs (Fig. S2G). The wound healing assay showed only 12.6% wound area remaining after 24 hours in the conditioned medium group as opposed to 40.4% in the control group (Fig. S2H-I), and this enhanced effect was also observed in EGM-2 condition as early as 8 hours (Fig. S4D-E). BMSC-CM treatment increased *MKI67* and *PCNA* gene expression (Fig. S2J), which is consistent with the Ki67 immunostaining and cell number count. Finally, elevated levels of proangiogenic genes including *VEGF, ANGPT1* and *ANGPT2* were detected after 24- and 72-hours following exposure to the BMSC-CM (Fig. S2J, and Fig. S4F). Taken together, these experiments confirm the paracrine effect of BMSCs on endothelial cells enhances angiogenesis.

3.3. A Microfluidic platform establishes endothelial cell culture under hypoxia

Given that vascular endothelial cells are continually exposed to blood flow, and fluid forces have been shown to play critical roles in physiological processes [38,39], we hypothesized that culturing endothelial cells under flow in a hypoxic microenvironment is a better representation of the *in vivo* situation. To understand the role of blood flow-mimicking shear stress and dynamic cell-cell communication during vessel repair, we developed a microfluidic culture platform. We applied 0.5 µl/min flow rate through the vascular channel to mimic physiological levels of fluid shear stress [38,40].

Tile scans along the microfluidic channel revealed the formation of an endothelial monolayer onto the fibronectin-coated substrate (Fig. 3A). Live-dead staining 48 hours after seeding indicated very limited cell death (Fig. 3B). Confocal immunofluorescence microscopic analyses revealed the endothelial cell marker vWF and cell-cell adhesion proteins such as VE-Cadherin and PECAM-1 along their membranes (Fig. 3B). Induced SMAD2/3 and YAP nuclear translocation were observed in both control and BMSC-CM groups (Fig. 3C and 3E). Using qPCR, two direct SMAD2/3 target genes, *SMAD6* and *HESI* [41], were dramatically upregulated in the presence of fluid flow (Fig. 3D). Assessment of *CCN1* and *CCN2* expression confirmed the expected activation of the YAP signaling pathway in dynamic cultures (Fig. 3F). We next studied the proliferative behavior of endothelial cells in this dynamic system. BMSC-CM treatment significantly enhanced cell proliferation in HUVECs and HAECs at 24 hours, as shown by Ki67 immunostaining (Fig. 3G-H and Fig. S3, respectively). Overall, we have set up a dynamic microfluidic cell culture model in a physiologically relevant manner with excellent cell viability that enables us to study the interplay of biomechanical and biochemical signals and of endothelial and mesenchymal cells as an *in vitro* proxy of the fracture healing process

3.4. Microfluidic flow influences endothelial cell morphology independent of BMSC-CM under hypoxia

Endothelial cells exhibit changes in cell shape, cytoskeletal remodeling and gene expression in response to shear stress [42], but the effect of fluidic flow on endothelial morphology in combination with BMSC-CM has yet to be determined. To achieve this, we adapted flow rates to 3 µl/min in the single channel chip and assessed morphological changes following exposure to conditioned medium. We also involved static chip cultures in this experiment

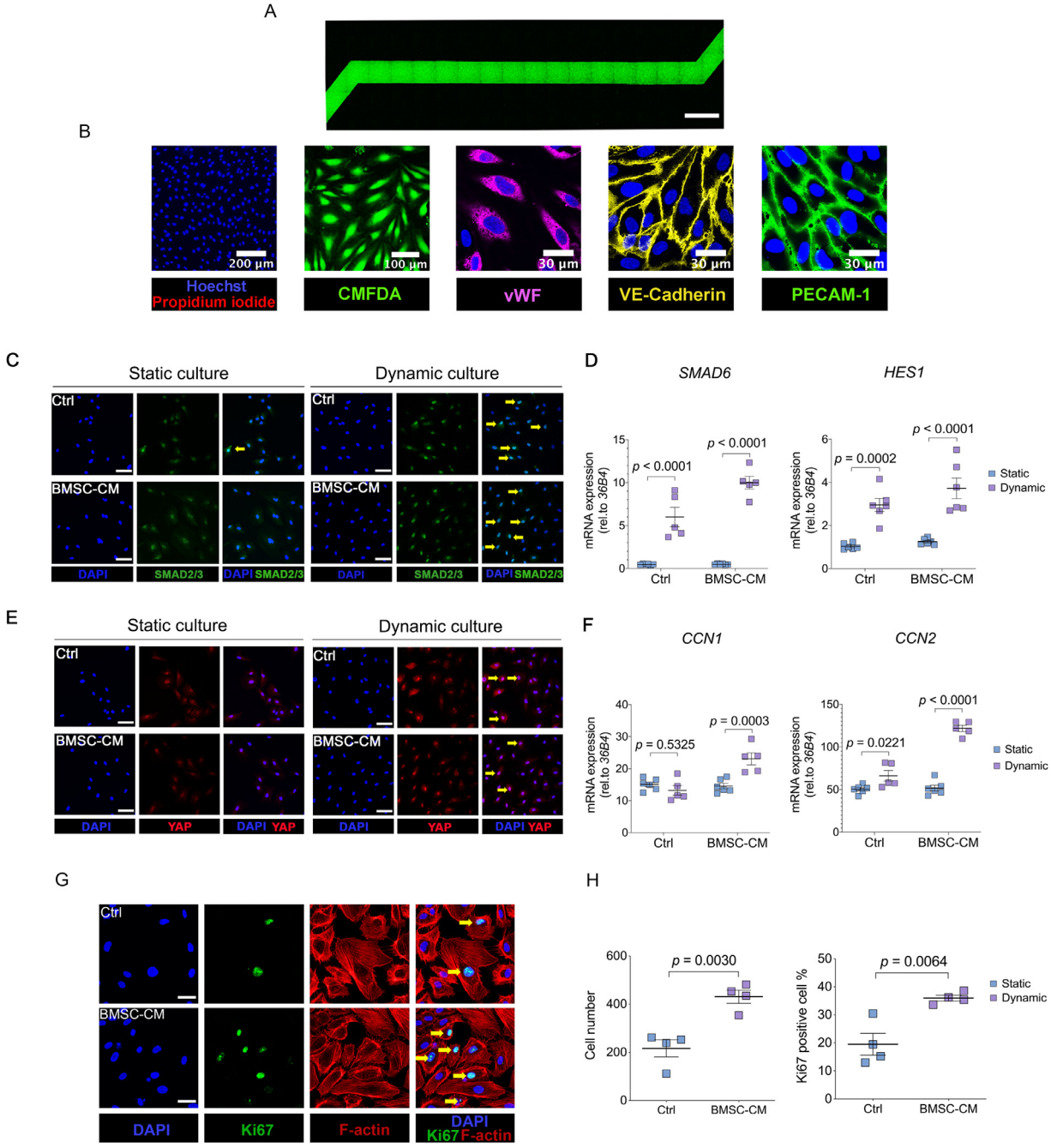

Fig. 3. Reconstitution of human endothelial cell culture in a microfluidic device. A Tile scan of the entire channel showing confluent HUVECs are cultured in the channel of microfluidic device. Cells are stained with a green cell tracker (CMFDA). **B** Representative images of HUVECs stained with Hoechst (live) and Propidium iodide (dead) viability staining kit on day 2. Live cells were stained blue while dead cells were stained red. Immunostaining micrographs of HUVECs cultured in microfluidic chips for 3 days labeled with CMFDA, vWF, VE-Cadherin and PECAM-1. **C** Representative images of SMAD2/3 immunostaining in endothelial cells after 24h treatment with BMSC-CM in static cultures and microfluidic chips under hypoxia. **D** Gene expression of downstream targets of SMAD2/3. **E** Representative images of YAP immunostaining in endothelial cells after 24h in the presence or absence of BMSC-CM in static cultures and microfluidic chips under hypoxia. **F** Gene expression of downstream targets of YAP. **G-H** Representative images (**G**) and quantitative data (**H**) of DAPI staining and Ki67 immunostaining. HUVECs were treated with or without BMSC-CM in static culture and microfluidic chips for 24h under the condition of hypoxia. Data are presented as means ± SEM, n = 4-6 independent microfluidic chips. **D-F** Analysis by two-way ANOVA followed by Šidák post hoc testing. **H** Analysis by Two-sided Student's t-test. Arrows indicate nuclear translocation (**C** and **E**) or Ki67 positive cells (**G**). **A** scale bar: 2000 µm, **C, E, G:** scale bars: 200 µm.

to determine flow-mediated cell shape changes. However, probably due to insufficient supply of nutrients in the microchannel, we observed many dead cells in static chip cultures after 48 hours of seeding (data not shown). Another important parameter that needs to be considered is the integrity of the endothelial monolayer, which is maintained by junctional structures. Of note, some junction proteins like VE-Cadherin were exclusively expressed at the cell borders not until 18 hours after seeding [43]. Therefore, we decided to allow the cells to form the monolayer for 24 hours before applying fluid flow for 12 hours (Fig. 4A).

HUVECs in the static conditions developed a rounded cobblestone morphology, and endothelial cells in the microfluidic chips were elongated and gently aligned with their major axis in the direction of the fluid flow as visualized by VE-Cadherin stain-

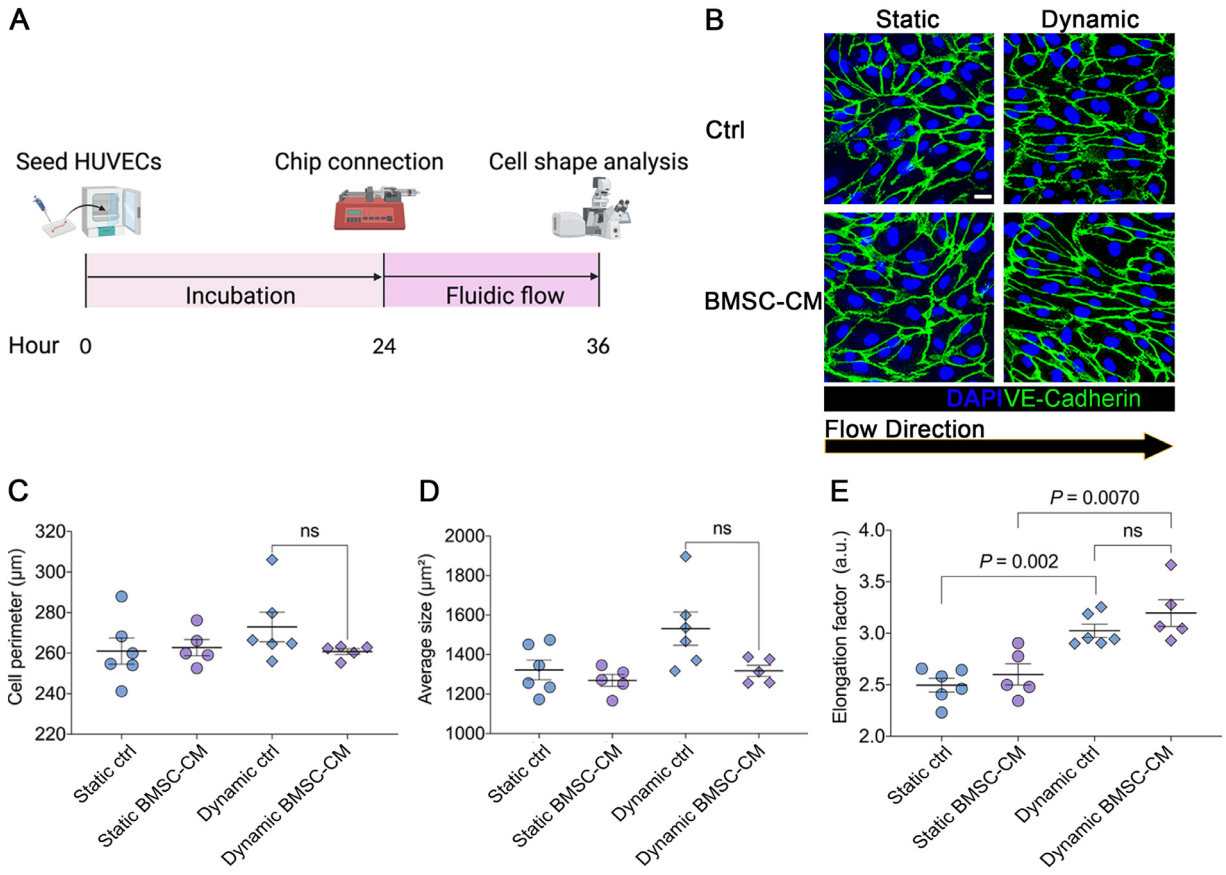

Fig. 4. Shear stress-induced morphological changes is independent of BMSC-CM. A Timeline for HUVEC seeding and cell shape analysis in microfluidic chips. **B** Immunostaining of VE-Cadherin showing shear stress induced endothelial cell alignment after 12 hours. **C-E** Quantification of endothelial cell shape parameters: cell perimeter (**C**) cell surface area (**D**) and cell elongation (**E**) in the presence of BMSC-CM or basal medium. Two-sided Student's *t*-test was used to analyze data in **C** and **D. E** Analysis by one-way ANOVA followed by Šidák post hoc testing. Data are presented as means ± SEM, 5-6 independent microfluidic chips were used in statistical analysis. Scale bar:100 μm.

ing (Fig. 4B). However, there was no difference in morphological changes with regard to cell perimeter and cell area between the control and BMSC-CM groups (Fig. 4C-D). Moreover, HUVECs in conditioned medium elongated to the same extent as for the control group (Fig. 4E). Together, these results show that cell shape changes are driven by shear stress in the microfluidic chips and occur independently of exogenous factors secreted by BMSCs.

3.5. Microfluidic wound healing model to study endothelial cell migration under hypoxia

Conventional migration models such as scratch assays and Boyden chamber assays are widely used methods in investigating cell migration. However, deeper insight into the *in vivo* function of endothelial cells requires a more suitable model that encompasses *in vivo* pathological elements such as blood vessel damage, flow dynamics and hypoxia into account. Therefore, we designed a second chip with 3 inlets that allows for independent and parallel fluid streams to flow over the cells [43]. Subsequent introduction of trypsin in the middle stream caused detachment of cells mimicking a 'damaged vessel' (Fig. 5A-B). As shown in Fig. 5B, endothelial cells in contact with trypsin were detached from the surfaces, while the untreated area flushed with EBM-2 on the sides remained intact. Moreover, the laminar flow resulted in negligible mixing among streams as shown by the sharp wound edge and formed a clear area enabling quantifying cell migration induced by a stimulus, without damaging cells on the leading edge, something that is difficult to avoid by physical scraping.

Once the wound had been generated, we reduced the total flow rate to 3 μl/min allowing mixing between adjacent streams to determine the profile of gradient growth factors in BMSC-CM (Fig. 5C). Differently sized fluorescent-labeled dextrans (10 and 40 kDa) in order to recapitulate the diffusion range of BMSC-CM derived growth factors were added to the middle stream. By checking the diffusion pattern and plotting the intensity of FITC-labelled dextrans, the shapes of the diffusion gradients for BMSC-CM were characterized (Fig. 5D). Collectively, these data demonstrate the microfluidic wound healing model is a promising tool to study endothelial cell migration and test the impact of additional stimuli.

3.6. BMSC-CM alters migratory behavior of endothelial cells toward damage in microfluidic chips

Endothelial cell migration during angiogenesis is the integrated resultant of external stimuli. Such stimuli can be mechanical forces which guide the random migration or chemotactic signals, which direct migratory process, towards a gradient of soluble chemoattractants (Fig. 6A). To investigate this process more thoroughly, we examined cellular responses in a well-controlled microfluidic chip in which we provided stable chemotactic concentrations (Fig. 6B). As expected, BMSC-CM provided stronger chemotactic recruitment of HUVECs indicated by a reduced wound area at 6 hours compared to control (Fig. 6C). To record real-time migratory characteristics, time-lapse imaging was applied to track individual cell movement (Movie S1). HUVECs subjected to control medium showed random movement with no directed migration

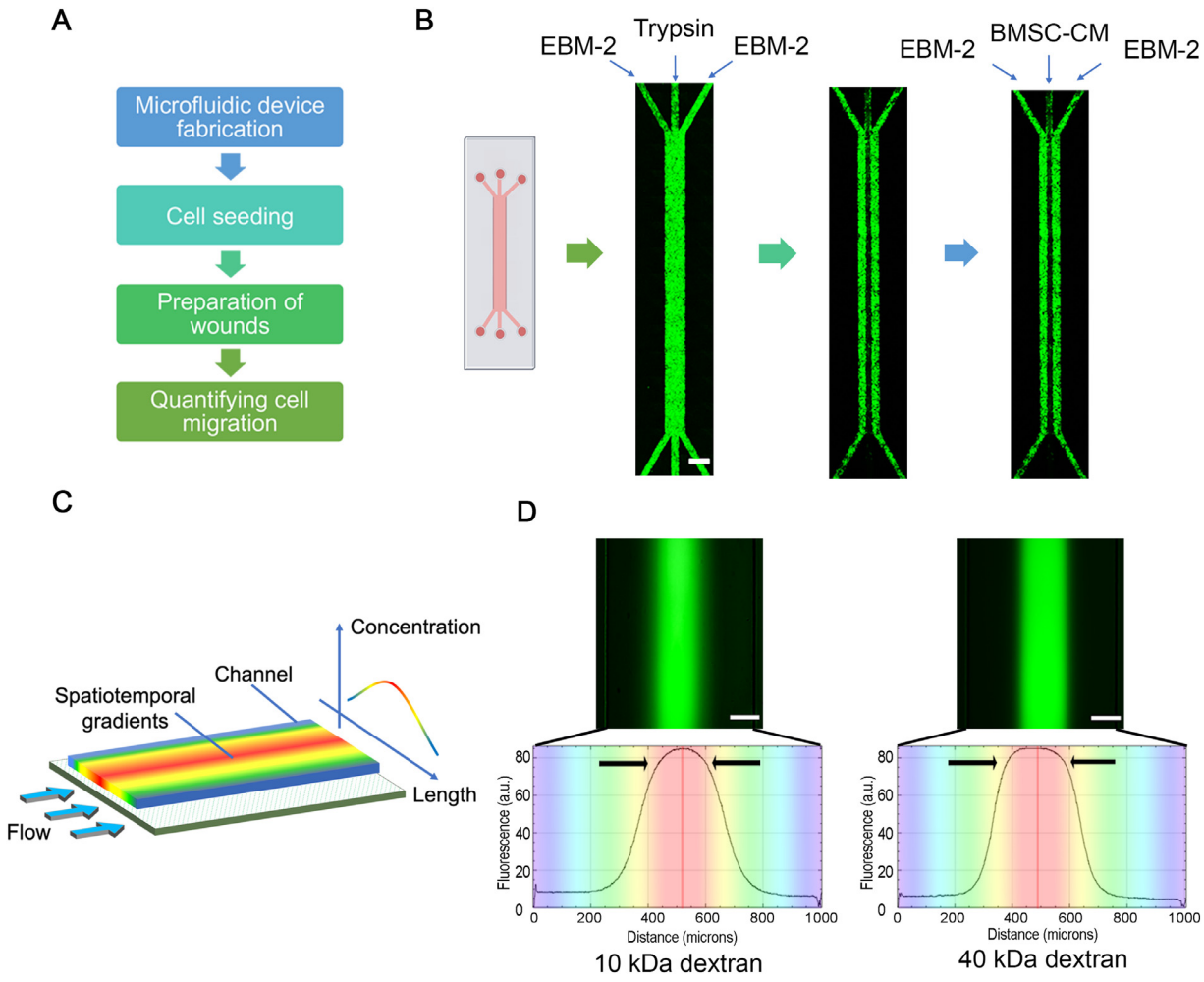

Fig. 5. Generation of microfluidic migration model. A Step-by-step illustrated procedure showing the generation of the microfluidic migration model. **B** Steps of wound generation in an endothelial monolayer. A wound was prepared by treating an endothelial monolayer with parallel streams containing EBM-2 (supplemented with 2% FCS) and trypsin. **C** Stable BMSC-CM gradient perpendicular to the flow. Two side streams parallel to the middle stream with a relatively low flow rate (3 µl/min) maintained the spatiotemporal gradient. **D** Fluorescent images of a microchannel infused with FITC-labeled 10-kDa dextran or 40-kDa dextran in the middle stream and PBS in the side streams. Relative concentrations were indicated as fluorescence intensities measured by drawing a line across the lateral position in the fluorescent images. The red line in the middle indicates the highest concentration. **B** scale bar: 1000 µm, **D** scale bar: 200 µm.

(Rayleigh test $p = 0.82$; Fig. 6D). In contrast, there was a significantly enhanced directed migration towards the growth factors in conditioned medium (Rayleigh test $p < 0.001$; Fig. 6D), implicating chemotaxis in the microfluidic chip.

To further elucidate the influence of BMSC-CM (causing a gradient density) on HUVEC migration, several relevant chemotaxis parameters were calculated according to the individual cell migration trajectories. For forward migration index (FMI) calculation, the x-axis refers to the direction parallel to the gradient density, while the y-axis refers to the direction perpendicular to the gradient density (= direction of the flow). As shown in Fig. 6D-E, HUVECs moved randomly without a preferential direction in an environment without BMSC-CM. In the presence of BMSC-CM, most cells moved directly towards the higher gradient density of cytokines (Fig. 6D-E). Additionally, higher velocity of HUVEC movement in the conditioned medium group (Fig. 6F) resulted in an accelerated wound healing capacity towards damage, consistent with the findings shown in Fig. 6C.

Shear stress can be sensed by endothelial cells, resulting in mechanical force-induced cell migration [44]. To investigate the role of BMSC-CM in this process, we switched the gradient infusion microfluidic model (Fig. 6B) to a design in which all three streams within the channel were identical, thereby creating a homogenous environment (Fig. 6G). Migration of HUVECs toward the damage region of the channel was observed as early as 6 hours, when exposed to shear stress in dynamic cultures (Fig. 6H). Importantly, the effect of BMSC-CM on endothelial cell migration led to a significantly smaller wound area in the dynamic compared to static cultures (Fig. 6H). Collectively, these data indicate the profound influences of BMSC-CM and fluid flow on endothelial cells, and further demonstrate that biomechanical and biochemical signals synergistically promote cell migration.

3.7. BMSC-CM changes transcriptional profiles of endothelial cell in both static and dynamic conditions

To define the biologic significance of the dynamic culture-induced findings, we performed transcriptome sequencing on endothelial cells under the treatment of BMSC-CM in both static cultures and microfluidics-based single channel chips. A direct comparison of mRNA expression profiles in BMSC-CM treated endothelial cells versus control in dynamic cultures revealed a total of 825 differentially expressed genes (DEGs) of which 200 were upregulated and 625 were downregulated (Fig. 7A). In contrast, there were only 21 upregulated and 42 downregulated genes in BMSC-CM compared to the control group in static cultures (Fig. 7A). Remarkably, the application of shear stress induced 3013 (1408 up and 1605 down) and 366 (207 up and 159 down) DEGs in the

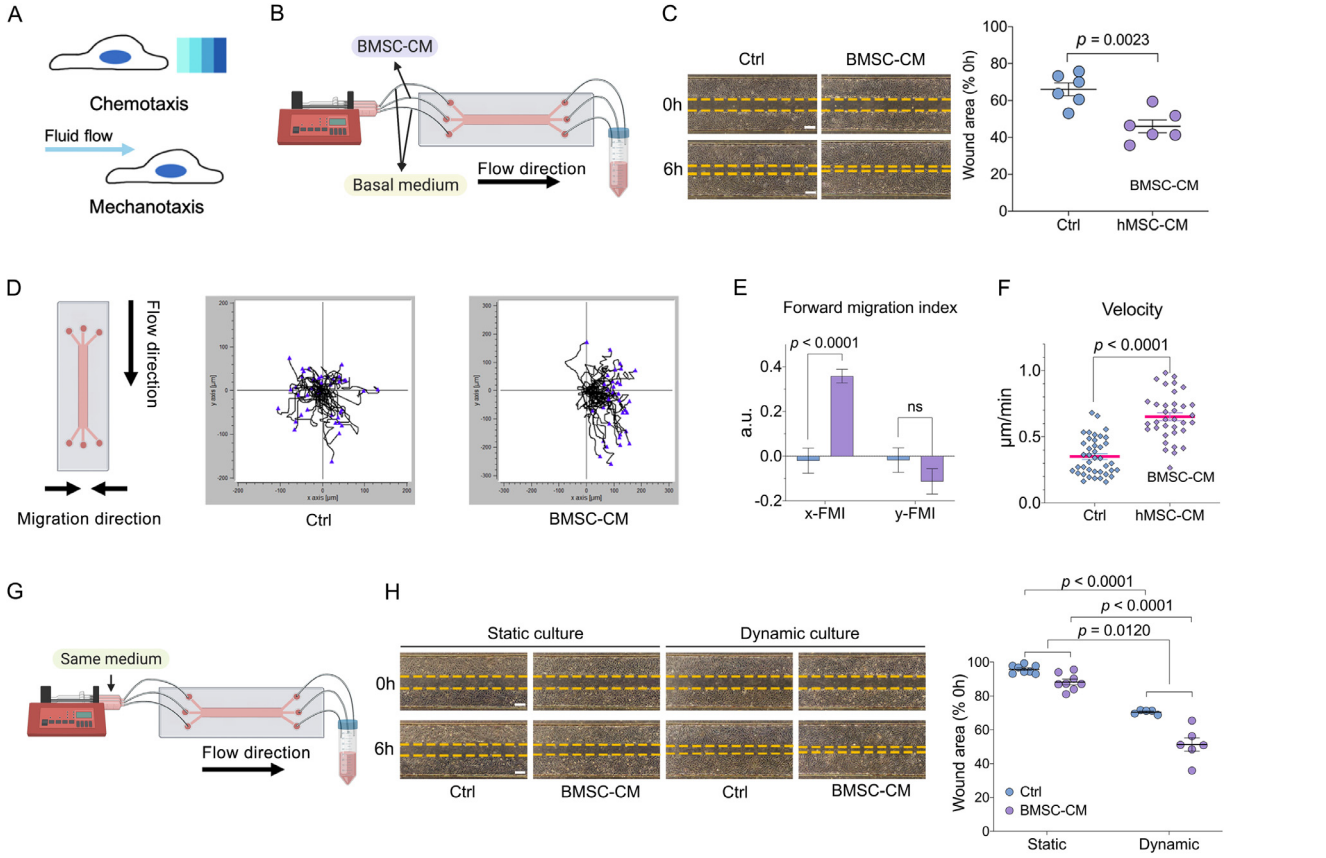

Fig. 6. BMSC-CM alters migration behavior of endothelial cells in microfluidic chips. A A schematic diagram showing types of stimuli of cell migration. **B** A schematic diagram showing the set-up of migration model used in (**c**). Both basal medium group and BMSC-CM group are supplemented with 2% FCS. **C** Representative images and quantitative analysis showing cell migration in the presence or absence of BMSC-CM gradient density after 6 hours. 6 independent microfluidic chips were used in statistical analysis, and two-sided Student's *t*-test was used to analyze data. **D** Representative migration trajectories of HUVECs exposed to BMSC-CM gradient density after 8 hours in microfluidic chips. Cell migration trajectories from left to middle were recorded. The initial position was defined as the 0 point in the X-Y plane, and cell tracks (40 tracks were used in control group, and 35 tracks were used in BMSC-CM group) in sequential images were plotted. **E-F** Quantification of forward migration index (FMI, **E**), and velocity (**F**) using 35-40 cell tracks from time-lapse imaging. FMI parallel to BMSC-CM gradient density was defined as x-FMI, while FMI perpendicular to BMSC-CM gradient was defined as y-FMI. **E** Analysis by two-way ANOVA followed by Šidák post hoc testing. Two-sided Student's *t*-test was used to analyze **F. G** A schematic diagram showing the set-up of migration model used in (**H**). **H** Representative images and quantitative analysis of cell migration in response to BMSC-CM in microfluidic chips. The dataset and the interaction between BMSC-CM and dynamic condition was analyzed using two-way ANOVA. 5-8 independent microfluidic chips were used in statistical analysis. Data are presented as means ± SEM. Scale bars: 200 μm.

presence or absence of BMSC-CM, respectively (Fig. 7A), illustrating the fact that BMSC-CM treatment combined with shear stress induces around 10-fold (3013 vs. 366) increase in DEGs. Most interestingly, BMSC-CM in the dynamic condition led to a more than 13-fold (825 vs. 63) DEGs increase compared to the static culture (Fig. 7A), indicating the crosstalk and synergistic action of BMSC-CM and shear stress in regulating transcriptional signatures.

Principal component analysis (PCA) supported the clustering of biological replicates and segregation of each population (Fig. 7B-C). In response to BMSC-CM, endothelial cells displayed enrichments for the VEGF pathway (Fig. 7D-E), as well as transcriptional signatures of angiogenesis stimulatory signals (Fig.S5A), including Hedgehog and *Myc* pathways [45,46] in both static and dynamic cultures, further supporting the functional data (Fig.S5B).

3.8. Dynamic cultures exposed to BMSC-CM are enriched in processes related to glycolysis, fatty acid metabolism and oxidative phosphorylation

Gene ontology (GO) analyses revealed regulated biological processes shared among all four comparisons and these terms are associated with signatures such as response to stimulus, lipid metabolic process, whereas endothelial cell related signatures such as vasculogenesis/angiogenesis, endothelial cell proliferation and migration are shared between 2 or more comparisons (Fig. 8A-D and data file S1). Notably, comparison of BMSC-CM in dynamic versus its static culture conditions exclusively demonstrated signatures related to ATP metabolic process, mitochondrial function and oxidative phosphorylation (Fig. 8D). Enrichment of transcriptional signatures in glycolysis, fatty acid metabolism and oxidative phosphorylation were identified when comparing BMSC-CM in dynamic cultures to either BMSC-CM in static cultures (Fig. 8E-G) or with control medium in dynamic cultures (Fig.S6). Moreover, several genes such as IDHs, SUCLs, SDHs, FH and MDHs, constituting essential components of the tricarboxylic acid (TCA) cycle, were strongly up-regulated in endothelial cells exposed to BMSC-CM in dynamic compared to static cultures (Fig. 8H), whereas only one of these genes was up-regulated in dynamic controls versus those static samples (Fig.S7A). On the other hand, BMSC-CM samples in the dynamic cultures enhanced approximately half of the TCA cycle-involved genes compared to only a few in controls (Fig.S7B). These observations were further confirmed by qPCR analyses (Fig.S8). Collectively, these transcriptional profiles indicate that energy metabolism is strongly involved in the response of endothelial cells exposed to a combination of BMSC-CM and shear stress.

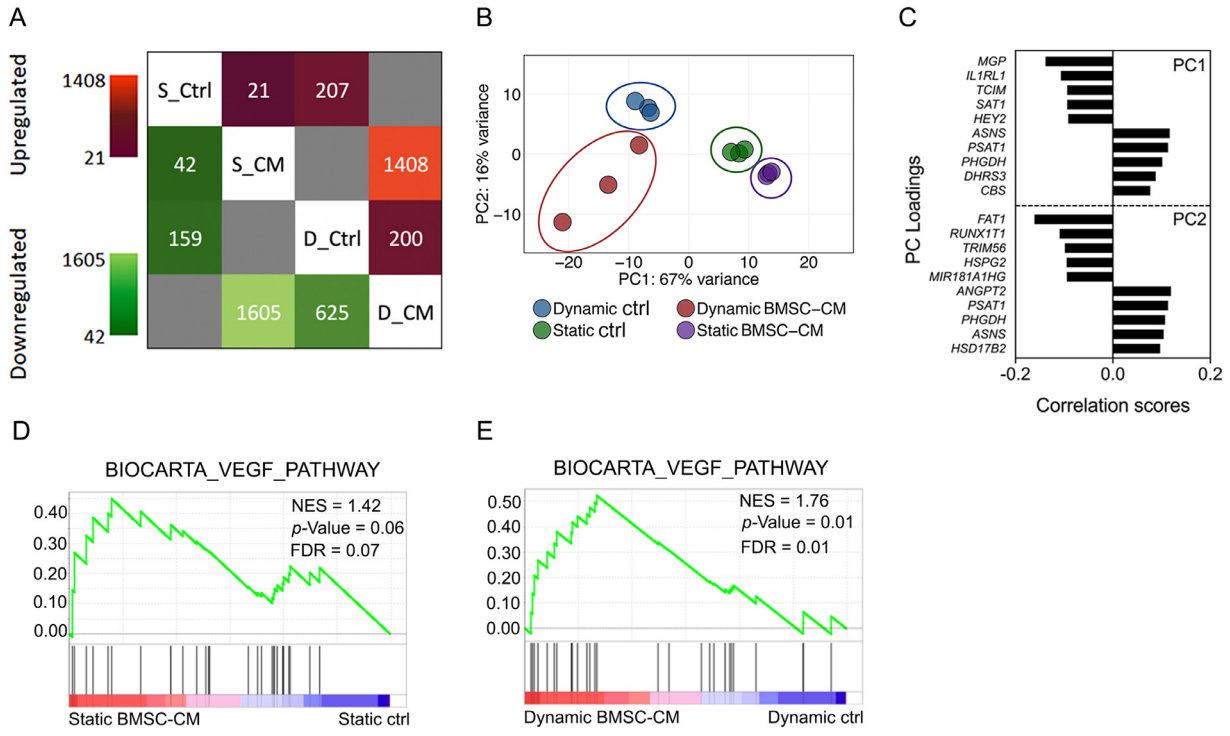

Fig. 7. Transcriptomic profiles of HUVECs exposed to BMSC-CM in static culture and dynamic cultures.
A Heatmap showing the number of differentially expressed genes (DEGs) of HUVECs response to control medium (Ctrl) and BMSC-CM in static (S) and dynamic (D) cultures. Adjusted $p < 0.05$ and Log_2 fold change ≥ 1. **B-C** Principal component analysis (PCA, **B**) and correlation scores of the top ten genes driving PC1 and PC2 in (**C**). **D-E** Transcriptional landscapes indicative of increased VEGF pathway in static (**D**) and dynamic (**E**) conditions exposed to BMSC-CM. NES: normalized enrichment score. FDR: false discovery rate.

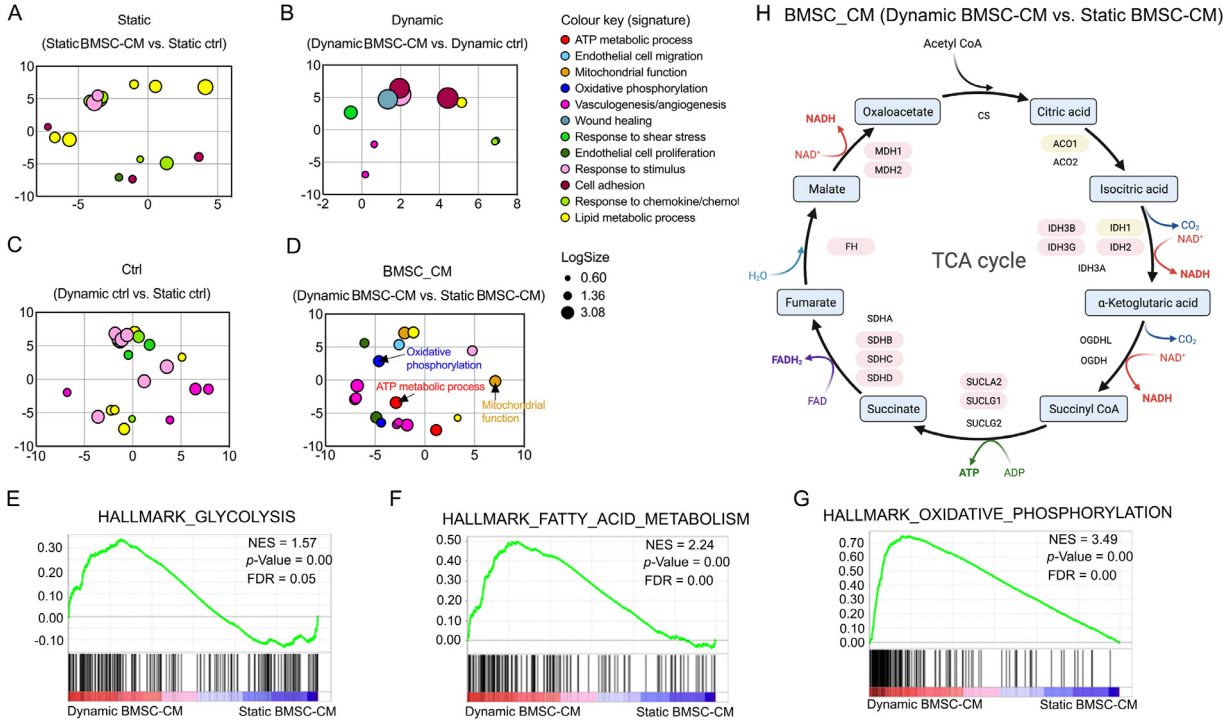

Fig. 8. Dynamic cultures exposed to BMSC-CM are enriched in processes related to glycolysis, fatty acid metabolism and oxidative phosphorylation. A-D Biological process-enriched DEGs in gene ontology (GO) analysis during static culture (**A**) and dynamic culture (**B**) exposed to control medium (Ctrl, **C**) and BMSC-CM (**D**). GO terms were summarized and trimmed using REVIGO to have a representative subset of the terms (signatures). In these scatterplots, x and y coordinates were derived by applying multidimensional scaling to a matrix of the GO terms' semantic similarities. The proximity of dots on the plots reflects the closeness in semantics of GO terms. GO terms in a relevant signature are indicated with the same color. Arrows indicate the unique signatures exclusively found in the comparison of dynamic BMSC-CM vs. static BMSC-CM. **E-G** Transcriptional landscapes indicative of increased glycolysis (**E**), fatty acid metabolism (**F**) and oxidative phosphorylation (**G**). **H** Altered genes in tricarboxylic acid (TCA) cycle of BMSC-CM in dynamic versus static condition. Significant changes of transcriptional profiles between dynamic BMSC-CM and static BMSC-CM groups are indicated. Upregulated transcripts are given in red, downregulated transcripts are given in yellow. NES: normalized enrichment score, FDR: false discovery rate.

4. Discussion

The present study characterizes the angiogenic features of BMSC-CM under hypoxia in dynamic cultures and shows the potential metabolism reprogramming in angiogenesis under BMSC-derived biochemical signals and biomechanical stimulation. The two well-controlled microfluidic designs were applied that permit analyses of key steps during angiogenesis, as well as analyses of chemotactic and mechanotactic-based cell migration mechanisms in response to a myriad of bioactive factors. The application of BMSC-CM in dynamic cultures shows that growth factors in combination with shear stress stimulated endothelial cell migration compared to either condition alone, demonstrating synergistic effects on angiogenesis during vessel repair. In addition, transcriptome analyses shows that BMSC-CM facilitates shear stress-regulated gene expression and provides insights into the role of metabolic adaptation during angiogenesis. Both findings stress the importance of studying endothelial cell function in the context of both biomechanical and biochemical signals, and further provide thoughts in developing therapeutic methods for fracture healing.

A number of studies have reported the co-culture of MSCs and endothelial cells using microfluidic approaches, but they either fail to introduce continuous flow which is the essential element for mimicking *in vivo* - like microenvironment [47–52], or focus on the differentiation and migration of MSCs [53,54]. Another co-culture model was developed as a potential tool for drug testing in which MSCs were cultured as three-dimensional aggregates in contact with endothelial cells [55]. However, this study focused on adhesion and marker expression such as CD31 and vWF of endothelial cells instead of angiogenesis or vessel function. Other self-organized co-culture models showed the stabilizing effect of MSCs on the formation of microvascular networks, but this study was performed in a normoxic environment that is different from the situation upon vessel damage [56,57]. The advantage of our current setting is the ability to integrate the essential elements for vessel repair in culture [58] where endothelial cells simultaneously experience dynamic flow under hypoxia and are exposed trophic factors from BMSCs, which enabled us to deeply investigate the interaction of biomechanical and biochemical signals.

Tissue origin of MSC secretome has shown dissimilarities with respect to their angiogenic profile [59], and the appropriate therapeutic use of MSC secretomes greatly depends on the perspective of specific clinical questions. For bone repair purposes, we employed human bone marrow-derived MSCs, which have been described to possess an increased angiogenic potential [59]. The hypoxic precondition of BMSCs we applied was inspired by the observation that blood vessel disruption leads to decreased oxygen supply, which stimulates the secretion of growth factors and cytokines released by MSCs [60,61]. Although trophic factors and extracellular vesicles (EVs) are broadly defined as the cell secretome, studies have demonstrated that EVs secreted by MSCs are less sensitive than conditioned medium in the context of angiogenesis [62,63]. By analyzing the composition of the hypoxia-activated MSC secretome, the current study demonstrated that a wide range of angiogenesis-related proteins are secreted by BMSCs. Consistent with previous reports [18,64,65], our data shows that BMSC-CM is able to trigger pronounced angiogenic responses including cell adhesion, proliferation and migration in basic culture condition (EBM-2) and in some cases even stronger than observed in the supposed optimal culture environment (EGM-2) containing abundant growth factors.

Conventional static cell culture used in investigating the paracrine function of BMSCs on endothelial cells have yielded a great deal of insights into underlying mechanisms governing angiogenesis [66–68]. However, these static cell cultures limitedly reflect the situation at the fracture site, as fluid shear stress is crucial to accurately mimic the repair process. To address the limitations in static cell cultures, we applied BMSC-CM into microfluidic chips with accurately controlled shear stress in a hypoxia-mimicking environment. Exposing HUVECs to $CoCl_2$, a HIF1α-inducing mimetic, not only mimics decreased oxygen level during vessel disruption in static cultures but also paves the way for employing hypoxia environment in microfluidic system without the need for specialized hypoxic culture chambers. Given the evidence that perfusion is decreased at a fracture site and blood vessel recovery from damage is accompanied by very minimal flow [40,69], we therefore applied shear stress as low as 0.04 dyne/cm^2 in microfluidic devices to mimic the key angiogenic steps *in vivo.* Endothelial cells showed an increased proliferation rate when exposed to shear stress in dynamic cultures. Moreover, we found support for activation of the YAP and SMAD signaling pathway upon shear stress by increased expression of downstream genes, irrespective of the presence of growth factors. The translation from mechanical signals to a biological response is probably mediated by multiple mechanoreceptors such as PECAM-1/VE-Cadherin/VEGFR2 [70]. One possible explanation for the enhanced proliferation triggered by BMSC-CM in the presence of shear stress is the activation of mechanosignaling pathways resulting in increased response by endothelial cells to growth factors. Alternatively, shear stress and MSC-derived growth factors may converge on common downstream pathways to play a synergistic role on cell proliferation. These observations indicate the importance of biologically relevant shear stress on endothelial cell behavior.

A microfluidic-based assay was developed as a tool to investigate directional migration by applying chemoattractants on endothelial cells under continuous flow [43]. We therefore generated a BMSC-CM gradient through the channel on both sides of the wound and applied a relatively low flow rate (3 µl/min) allowing for diffusion between adjacent streams. HUVECs exposed to the gradient environment of BMSC-CM revealed the expected directed migration (Fig. 6C-D), but failed to show enhanced migratory behavior compared to cells cultured in a homogeneous BMSC-CM environment at 6 hours (Fig. 6H). This can be explained by desensitization of G-coupled receptor kinase-mediated receptor signaling [71], suggesting the requirement for a rising chemoattractant concentration to prompt a prolonged response. The participation of VEGF in endothelial cells recruitment is critical to vessel recovery and fracture healing. Moreover, cellular sensing to a stable VEGFA gradient has been reported to chemotactically induce migratory behavior [72]. However, even when using this most potent proangiogenic factor, there is no conclusive benefit of revascularization using VEGF therapy [73], further implicating the importance of using a combination therapy under fluid flow in combination with growth factors for maximum efficacy.

Exposure of endothelial cells to fluid flow resulted in cellular alignment and elongation through focal adhesion-regulation and cytoskeletal organization [74]. Consistent with previous research [75], our data indicate that shear stress is a dominant factor in determining morphological responses regardless of exogenous supplements. Moreover, the migratory response was strongly augmented under fluid flow compared to static cultures undergoing identical BMSC-CM treatment, underscoring the synergistic benefit of shear stress and BMSC-derived growth factors. Potentially, the shear stress-transmitted signal sensed by luminal membranes and its receptors thereon activates focal adhesions, which contribute to mitogenic signaling pathways in an outside-in and inside-out manner, while influencing chemotactic cell migration [76].

To provide further insights explaining the observed effect of BMSC-CM and shear stress on endothelial cells, we performed gene expression profiling analyses. A large number of DEGs were retrieved from the combination of BMSC-CM and shear stress treat-

ment samples compared to either treatment alone, further supporting a synergistic action of biochemical and biomechanical cues in regulating endothelial cell behavior. In addition, our findings implicate that BMSC-CM together with shear stress significantly alters the metabolic character of endothelial cells as shown by the activation of glycolysis, fatty acid oxidation and oxidative phosphorylation. A key function of oxidative phosphorylation is to sustain biosynthetic processes instead of ATP production (endothelial cells meet energy demand mainly through glycolysis) [77–79]. The enhanced proliferation and migration of endothelial cells induced by combined BMSC-CM and shear stress are probably the result of activated biosynthetic processes. Blockade of complexes I and III in the electron transport chain impairs endothelial cell proliferation, demonstrating the critical role of oxidative phosphorylation in angiogenesis [77]. Moreover, we observed upregulation of specific genes in the TCA cycle in dynamic cultures exposed to BMSC-CM. This will result in abundant production of its intermediates, which serves as substrates essential for endothelial cell proliferation [77]. Collectively, our observations are consistent with the recognition that endothelial cell metabolism drives angiogenesis in parallel with pro-angiogenic factors [80].

In the current study we identified two limitations. We did not utilize human bone marrow-derived endothelial cells, especially $CD31^+$ $EMCN^+$ cells from Type-H capillaries, which are closely coupled to osteogenesis during fracture healing. Unfortunately, isolation of these cells needs an unrealistically large human sample size as they only account for 0.015% of the total bone marrow cell population and until very recently there was no optimal isolation method available [81]. Secondly, while the present microfluidic models provide us with potent and convenient tools to investigate complex signals during angiogenesis, advanced Organ-on-Chip models emulating the “fracture” integrated with inflammatory signals, hypoxia and shear stress should be developed to enable mimicking even more complex *in vivo* situations.

In conclusion, our results demonstrate the importance of recapitulating *in vivo* - like microenvironments when investigating key events during vessel repair. Endothelial cells exhibit enhanced angiogenesis characteristics when simultaneous exposing them to BMSC-CM, mechanical forces and biochemical signals simultaneously. The improved angiogenesis may not only result from the direct effect of growth factors, but also by reprogramming of endothelial cell metabolism. Moreover, with this model we demonstrated a synergistic impact of biomechanical and biochemical signaling on endothelial cell behavior and the expression of genes involved in the TCA cycle and energy metabolism, which opens an interesting avenue to stimulate angiogenesis during fracture healing. Future work will be essential to provide additional mechanistic insights into the metabolic adaptation of endothelial cells in physiological and pathological conditions, which should ultimately lead to tailor-made therapeutic strategies for fracture healing.

Funding

Shuang Zhang is supported by the China Scholarship Council through a PhD Research Fellowship Grant (No. 201709370052).

Author contributions

Shuang Zhang, Pouyan E. Boukany, Johan W. van Neck, Johannes P.T.M. van Leeuwen and Bram C.J. van der Eerden designed the studies. Shuang Zhang, Bastiaan Tuk, Marijke Koedam, Jeroen van de Peppel, Georg Pesch, Gert-Jan Kremers, Remco M. Hoogenboezem, Eric M. J. Bindels performed experiments and interpreted data. Shuang Zhang wrote the manuscript. All authors read and approved the manuscript.

Declaration of Competing Interest

The authors declare that they have no known competing financial interests or personal relationships that could have appeared to influence the work reported in this paper.

Acknowledgment

All schematic figures were created with BioRender.com.

Supplementary materials

Supplementary material associated with this article can be found, in the online version, at doi:10.1016/j.actbio.2022.08.025.

References

[1] G.N. Bancroft, A.G. Mikos, Bone tissue engineering by cell transplantation, in: R.L. Reis, D. Cohn (Eds.), Polymer Based Systems on Tissue Engineering, Replacement and Regeneration, Springer Netherlands, Dordrecht, 2002, pp. 251–263.
[2] L.A. Mills, S.A. Aitken, A. Simpson, The risk of non-union per fracture: current myths and revised figures from a population of over 4 million adults, Acta Orthop. 88 (4) (2017) 434–439.
[3] R. Zura, Z. Xiong, T. Einhorn, J.T. Watson, R.F. Ostrum, M.J. Prayson, G.J. Della Rocca, S. Mehta, T. McKinley, Z. Wang, R.G. Steen, Epidemiology of fracture nonunion in 18 human bones, JAMA Surg. 151 (11) (2016) e162775.
[4] M.A. Miranda, M.S. Moon, Treatment strategy for nonunions and malunions, Surg. Treat. Orthop. Trauma 1 (2007) 77–100.
[5] H.B. El-Zawawy, C.S. Gill, R.W. Wright, L.J. Sandell, Smoking delays chondrogenesis in a mouse model of closed tibial fracture healing, J. Orthop. Res. 24 (12) (2006) 2150–2158.
[6] L. Cozen, Does diabetes delay fracture healing? Clin. Orthop. Relat. Res. 82 (1972) 134–140.
[7] S.R. Smith, J.T. Bronk, P.J. Kelly, Effect of fracture fixation on cortical bone blood flow, J. Orthop. Res. 8 (4) (1990) 471–478.
[8] O. Grundnes, O. Reikerås, Blood flow and mechanical properties of healing bone. Femoral osteotomies studied in rats, Acta Orthop. Scand. 63 (5) (1992) 487–491.
[9] J. Glowacki, Angiogenesis in fracture repair, Clin. Orthopaed. Relat. Res.® 355 (1998) S82–S89.
[10] K.D. Hankenson, M. Dishowitz, C. Gray, M. Schenker, Angiogenesis in bone regeneration, Injury 42 (6) (2011) 556–561.
[11] T.A. Einhorn, L.C. Gerstenfeld, Fracture healing: mechanisms and interventions, Nat. Rev. Rheumatol. 11 (1) (2015) 45–54.
[12] F.W. Rhinelander, Tibial blood supply in relation to fracture healing, Clin. Orthop. Relat. Res. (105) (1974) 34–81.
[13] K. Schmidt-Bleek, H. Schell, N. Schulz, P. Hoff, C. Perka, F. Buttgereit, H.D. Volk, J. Lienau, G.N. Duda, Inflammatory phase of bone healing initiates the regenerative healing cascade, Cell Tissue Res. 347 (3) (2012) 567–573.
[14] B. Decker, H. Bartels, S. Decker, Relationships between endothelial cells, pericytes, and osteoblasts during bone formation in the sheep femur following implantation of tricalciumphosphate-ceramic, Anat. Rec. 242 (3) (1995) 310–320.
[15] M. Melnyk, T. Henke, L. Claes, P. Augat, Revascularisation during fracture healing with soft tissue injury, Arch. Orthop. Trauma Surg. 128 (10) (2008) 1159–1165.
[16] M.R. Hausman, M.B. Schaffler, R.J. Majeska, Prevention of fracture healing in rats by an inhibitor of angiogenesis, Bone 29 (6) (2001) 560–564.
[17] M. Komaki, Y. Numata, C. Morioka, I. Honda, M. Tooi, N. Yokoyama, H. Ayame, K. Iwasaki, A. Taki, N. Oshima, I. Morita, Exosomes of human placenta-derived mesenchymal stem cells stimulate angiogenesis, Stem Cell Res. Ther. 8 (1) (2017) 219.
[18] M.A. Gharaei, Y. Xue, K. Mustafa, S.A. Lie, I. Fristad, Human dental pulp stromal cell conditioned medium alters endothelial cell behavior, Stem Cell Res. Ther. 9 (1) (2018) 69.
[19] L. Liang, Z. Li, T. Ma, Z. Han, W. Du, J. Geng, H. Jia, M. Zhao, J. Wang, B. Zhang, J. Feng, L. Zhao, A. Rupin, Y. Wang, Z.C. Han, Transplantation of human placenta-derived mesenchymal stem cells alleviates critical limb ischemia in diabetic nude rats, Cell Transplant. 26 (1) (2017) 45–61.
[20] L. Liang, Prenatal mesenchymal stem cell secretome and its clinical implication, in: Z.C. Han, T.A. Takahashi, Z. Han, Z. Li (Eds.), Perinatal Stem Cells: Biology, Manufacturing and Translational Medicine, Springer Singapore, Singapore, 2019, pp. 167–173.
[21] R. Castellon, H.K. Hamdi, I. Sacerio, A.M. Aoki, M.C. Kenney, A.V. Ljubimov, Effects of angiogenic growth factor combinations on retinal endothelial cells, Exp. Eye Res. 74 (4) (2002) 523–535.
[22] S.K. Kim, J. Lee, M. Song, M. Kim, S.J. Hwang, H. Jang, Y. Park, Combination of three angiogenic growth factors has synergistic effects on sprouting of endothelial cell/mesenchymal stem cell-based spheroids in a 3D matrix, J. Biomed. Mater. Res. B Appl. Biomater. 104 (8) (2016) 1535–1543.

[23] A. Bronckaers, P. Hilkens, W. Martens, P. Gervois, J. Ratajczak, T. Struys, I. Lambrichts, Mesenchymal stem/stromal cells as a pharmacological and therapeutic approach to accelerate angiogenesis, Pharmacol. Ther. 143 (2) (2014) 181–196.
[24] E. Gordon, L. Schimmel, M. Frye, The importance of mechanical forces for in vitro endothelial cell biology, Front. Physiol. 11 (684) (2020).
[25] C. Bruedigam, M. Driel, M. Koedam, J. Peppel, B.C. van der Eerden, M. Eijken, J.P. van Leeuwen, Basic techniques in human mesenchymal stem cell cultures: differentiation into osteogenic and adipogenic lineages, genetic perturbations, and phenotypic analyses, Curr. Protoc. Stem Cell Biol. Chapter 1 (2011) Unit1H.3.
[26] F.A. Fierro, A.J. O'Neal, J.R. Beegle, M.N. Chávez, T.R. Peavy, R.R. Isseroff, J.T. Egaña, Hypoxic pre-conditioning increases the infiltration of endothelial cells into scaffolds for dermal regeneration pre-seeded with mesenchymal stem cells, Front. Cell Dev. Biol. 3 (68) (2015).
[27] T.-E. Park, N. Mustafaoglu, A. Herland, R. Hasselkus, R. Mannix, E.A. FitzGerald, R. Prantil-Baun, A. Watters, O. Henry, M. Benz, H. Sanchez, H.J. McCrea, L.C. Goumnerova, H.W. Song, S.P. Palecek, E. Shusta, D.E. Ingber, Hypoxia-enhanced Blood-Brain Barrier Chip recapitulates human barrier function and shuttling of drugs and antibodies, Nat. Commun. 10 (1) (2019) 2621.
[28] J. Schindelin, I. Arganda-Carreras, E. Frise, V. Kaynig, M. Longair, T. Pietzsch, S. Preibisch, C. Rueden, S. Saalfeld, B. Schmid, J.-Y. Tinevez, D.J. White, V. Hartenstein, K. Eliceiri, P. Tomancak, A. Cardona, Fiji: an open-source platform for biological-image analysis, Nat. Methods 9 (7) (2012) 676–682.
[29] D. Warde-Farley, S.L. Donaldson, O. Comes, K. Zuberi, R. Badrawi, P. Chao, M. Franz, C. Grouios, F. Kazi, C.T. Lopes, A. Maitland, S. Mostafavi, J. Montojo, Q. Shao, G. Wright, G.D. Bader, Q. Morris, The GeneMANIA prediction server: biological network integration for gene prioritization and predicting gene function, Nucleic Acids Res. 38 (suppl_2) (2010) W214–W220.
[30] A.M. Brum, J. van de Peppel, C.S. van der Leije, M. Schreuders-Koedam, M. Eijken, B.C. van der Eerden, J.P. van Leeuwen, Connectivity map-based discovery of parbendazole reveals targetable human osteogenic pathway, Proc. Natl. Acad. Sci. USA 112 (41) (2015) 12711–12716.
[31] M.I. Love, W. Huber, S. Anders, Moderated estimation of fold change and dispersion for RNA-seq data with DESeq2, Genome Biol. 15 (12) (2014) 1–21.
[32] M.E. Ritchie, B. Phipson, D. Wu, Y. Hu, C.W. Law, W. Shi, G.K. Smyth, limma powers differential expression analyses for RNA-sequencing and microarray studies, Nucleic Acids Res. 43 (7) (2015) e47-e47.
[33] F. Supek, M. Bošnjak, N. Škunca, T. Šmuc, REVIGO summarizes and visualizes long lists of gene ontology terms, PLoS One 6 (7) (2011) e21800.
[34] A. Subramanian, P. Tamayo, V.K. Mootha, S. Mukherjee, B.L. Ebert, M.A. Gillette, A. Paulovich, S.L. Pomeroy, T.R. Golub, E.S. Lander, J.P. Mesirov, Gene set enrichment analysis: a knowledge-based approach for interpreting genome-wide expression profiles, Proc. Natl. Acad. Sci. 102 (43) (2005) 15545.
[35] Y. Xia, G.M. Whitesides, Soft lithography, Angew. Chem. Int. Ed Engl. 37 (5) (1998) 550–575.
[36] M. Nouri-Goushki, M.J. Mirzaali, L. Angeloni, D. Fan, M. Minneboo, M.K. Ghatkesar, U. Staufer, L.E. Fratila-Apachitei, A.A. Zadpoor, 3D printing of large areas of highly ordered submicron patterns for modulating cell behavior, ACS Appl. Mater. Interfaces 12 (1) (2020) 200–208.
[37] P. Zengel, A. Nguyen-Hoang, C. Schildhammer, R. Zantl, V. Kahl, E. Horn, µ-Slide chemotaxis: a new chamber for long-term chemotaxis studies, BMC Cell Biol. 12 (2011) 21.
[38] M.G. Bixel, A.P. Kusumbe, S.K. Ramasamy, K.K. Sivaraj, S. Butz, D. Vestweber, R.H. Adams, Flow dynamics and HSPC homing in bone marrow microvessels, Cell Rep. 18 (7) (2017) 1804–1816.
[39] D.A. Chistiakov, A.N. Orekhov, Y.V. Bobryshev, Effects of shear stress on endothelial cells: go with the flow, Acta Physiol. 219 (2) (2017) 382–408.
[40] R.E. Tomlinson, M.J. Silva, Skeletal blood flow in bone repair and maintenance, Bone Res. 1 (4) (2013) 311–322.
[41] P.Y. Chen, L. Qin, G. Li, J. Malagon-Lopez, Z. Wang, S. Bergaya, S. Gujja, A.W. Caulk, S.I. Murtada, X. Zhang, Z.W. Zhuang, D.A. Rao, G. Wang, Z. Tobiasova, B. Jiang, R.R. Montgomery, L. Sun, H. Sun, E.A. Fisher, J.R. Gulcher, C. Fernandez-Hernando, J.D. Humphrey, G. Tellides, T.W. Chittenden, M. Simons, Smooth muscle cell reprogramming in aortic aneurysms, Cell Stem Cell 26 (4) (2020) 542-557.e11.
[42] E.A. Osborn, A. Rabodzey, J.C. Forbes Dewey, J.H. Hartwig, Endothelial actin cytoskeleton remodeling during mechanostimulation with fluid shear stress, Am. J. Physiol.-Cell Physiol. 290 (2) (2006) C444–C452.
[43] A.D. van der Meer, K. Vermeul, A.A. Poot, J. Feijen, I. Vermes, A microfluidic wound-healing assay for quantifying endothelial cell migration, Am. J. Physiol. Heart Circ. Physiol. 298 (2) (2010) H719–H725.
[44] S. Li, N.F. Huang, S. Hsu, Mechanotransduction in endothelial cell migration, J. Cell. Biochem. 96 (6) (2005) 1110–1126.
[45] C. Di Mauro, R. Rosa, V. D'Amato, P. Ciciola, A. Servetto, R. Marciano, R.C. Orsini, L. Formisano, S. De Falco, V. Cicatiello, M. Di Bonito, M. Cantile, F. Collina, A. Chambery, B.M. Veneziani, S. De Placido, R. Bianco, Hedgehog signalling pathway orchestrates angiogenesis in triple-negative breast cancers, Br. J. Cancer 116 (11) (2017) 1425–1435.
[46] K. Shchors, E. Shchors, F. Rostker, E.R. Lawlor, L. Brown-Swigart, G.I. Evan, The Myc-dependent angiogenic switch in tumors is mediated by interleukin 1beta, Genes Dev. 20 (18) (2006) 2527–2538.
[47] B. Carrion, C.P. Huang, C.M. Ghajar, S. Kachgal, E. Kniazeva, N.L. Jeon, A.J. Putnam, Recreating the perivascular niche ex vivo using a microfluidic approach, Biotechnol. Bioeng. 107 (6) (2010) 1020–1028.
[48] J.S. Jeon, S. Bersini, J.A. Whisler, M.B. Chen, G. Dubini, J.L. Charest, M. Moretti, R.D. Kamm, Generation of 3D functional microvascular networks with human mesenchymal stem cells in microfluidic systems, Integr. Biol. 6 (5) (2014) 555–563.
[49] C. Peticone, D.D.S. Thompson, N. Dimov, B. Jevans, N. Glass, M. Micheletti, J.C. Knowles, H.-W. Kim, J.J. Cooper-White, I.B. Wall, Characterisation of osteogenic and vascular responses of hMSCs to Ti-Co doped phosphate glass microspheres using a microfluidic perfusion platform, J. Tissue Eng. 11 (2020) 2041731420954712.
[50] M. Watanabe, R. Sudo, Establishment of an *in vitro* vascular anastomosis model in a microfluidic device, J. Biomech. Sci. Eng. 14 (3) (2019) 18-00521-18-00521.
[51] M. Watanabe, R. Sudo, Microfluidic device setting by coculturing endothelial cells and mesenchymal stem cells, in: D. Ribatti (Ed.), Vascular Morphogenesis: Methods and Protocols, Springer US, New York, NY, 2021, pp. 57–66.
[52] E.A. Margolis, D.S. Cleveland, Y.P. Kong, J.A. Beamish, W.Y. Wang, B.M. Baker, A.J. Putnam, Stromal cell identity modulates vascular morphogenesis in a microvasculature-on-a-chip platform, Lab Chip 21 (6) (2021) 1150–1163.
[53] S. Park, H. Jang, B.S. Kim, C. Hwang, G.S. Jeong, Y. Park, Directional migration of mesenchymal stem cells under an SDF-1α gradient on a microfluidic device, PLoS One 12 (9) (2017) e0184595.
[54] F.A. Saleh, M. Whyte, P.G. Genever, Effects of endothelial cells on human mesenchymal stem cell activity in a three-dimensional in vitro model, Eur. Cell Mater. 22 (2011) 242–257 discussion 257.
[55] O.F. Khan, M.D. Chamberlain, M.V. Sefton, Toward an in vitro vasculature: differentiation of mesenchymal stromal cells within an endothelial cell-seeded modular construct in a microfluidic flow chamber, Tissue Eng. Part A 18 (7-8) (2012) 744–756.
[56] K. Yamamoto, K. Tanimura, Y. Mabuchi, Y. Matsuzaki, S. Chung, R.D. Kamm, M. Ikeda, K. Tanishita, R. Sudo, The stabilization effect of mesenchymal stem cells on the formation of microvascular networks in a microfluidic device, J. Biomech. Sci. Eng. 8 (2) (2013) 114–128.
[57] A. Mykuliak, A. Yrjänäinen, A.J. Mäki, A. Gebraad, E. Lampela, M. Kääriäinen, T.K. Pakarinen, P. Kallio, S. Miettinen, H. Vuorenpää, Vasculogenic potency of bone marrow- and adipose tissue-derived mesenchymal stem/stromal cells results in differing vascular network phenotypes in a microfluidic chip, Front. Bioeng. Biotechnol. 10 (2022) 764237.
[58] S. Stucker, J. Chen, F.E. Watt, A.P. Kusumbe, Bone angiogenesis and vascular niche remodeling in stress, aging, and diseases, Front. Cell Dev. Biol. 8 (2020) 602269.
[59] D. Kehl, M. Generali, A. Mallone, M. Heller, A.-C. Uldry, P. Cheng, B. Gantenbein, S.P. Hoerstrup, B. Weber, Proteomic analysis of human mesenchymal stromal cell secretomes: a systematic comparison of the angiogenic potential, npj Regener. Med. 4 (1) (2019) 8.
[60] C.J. Cunningham, E. Redondo-Castro, S.M. Allan, The therapeutic potential of the mesenchymal stem cell secretome in ischaemic stroke, J. Cereb. Blood Flow Metab. 38 (8) (2018) 1276–1292.
[61] L. Liu, J. Gao, Y. Yuan, Q. Chang, Y. Liao, F. Lu, Hypoxia preconditioned human adipose derived mesenchymal stem cells enhance angiogenic potential via secretion of increased VEGF and bFGF, Cell Biol. Int. 37 (6) (2013) 551–560.
[62] C. Gorgun, D. Ceresa, R. Lesage, F. Villa, D. Reverberi, C. Balbi, S. Santamaria, K. Cortese, P. Malatesta, L. Geris, R. Quarto, R. Tasso, Dissecting the effects of preconditioning with inflammatory cytokines and hypoxia on the angiogenic potential of mesenchymal stromal cell (MSC)-derived soluble proteins and extracellular vesicles (EVs), Biomaterials 269 (2021) 120633.
[63] G. Merckx, B. Hosseinkhani, S. Kuypers, S. Deville, J. Irobi, I. Nelissen, L. Michiels, I. Lambrichts, A. Bronckaers, Angiogenic effects of human dental pulp and bone marrow-derived mesenchymal stromal cells and their extracellular vesicles, Cells 9 (2) (2020).
[64] W. Liu, L. Li, Y. Rong, D. Qian, J. Chen, Z. Zhou, Y. Luo, D. Jiang, L. Cheng, S. Zhao, F. Kong, J. Wang, Z. Zhou, T. Xu, F. Gong, Y. Huang, C. Gu, X. Zhao, J. Bai, F. Wang, W. Zhao, L. Zhang, X. Li, G. Yin, J. Fan, W. Cai, Hypoxic mesenchymal stem cell-derived exosomes promote bone fracture healing by the transfer of miR-126, Acta Biomater. 103 (2020) 196–212.
[65] J.M. Sorrell, M.A. Baber, A.I. Caplan, Influence of adult mesenchymal stem cells on in vitro vascular formation, Tissue Eng. Part A 15 (7) (2009) 1751–1761.
[66] C. Shen, P. Lie, T. Miao, M. Yu, Q. Lu, T. Feng, J. Li, T. Zu, X. Liu, H. Li, Conditioned medium from umbilical cord mesenchymal stem cells induces migration and angiogenesis, Mol. Med. Rep. 12 (1) (2015) 20–30.
[67] F. Böhrnsen, H. Schliephake, Supportive angiogenic and osteogenic differentiation of mesenchymal stromal cells and endothelial cells in monolayer and co-cultures, Int. J. Oral Sci. 8 (4) (2016) 223–230.
[68] I.A. Potapova, G.R. Gaudette, P.R. Brink, R.B. Robinson, M.R. Rosen, I.S. Cohen, S.V. Doronin, Mesenchymal stem cells support migration, extracellular matrix invasion, proliferation, and survival of endothelial cells in vitro, Stem Cells 25 (7) (2007) 1761–1768.
[69] J.Y. Park, J.B. White, N. Walker, C.-H. Kuo, W. Cha, M.E. Meyerhoff, S. Takayama, Responses of endothelial cells to extremely slow flows, Biomicrofluidics 5 (2) (2011) 22211-22211.
[70] E. Tzima, M. Irani-Tehrani, W.B. Kiosses, E. Dejana, D.A. Schultz, B. Engelhardt, G. Cao, H. DeLisser, M.A. Schwartz, A mechanosensory complex that mediates the endothelial cell response to fluid shear stress, Nature 437 (7057) (2005) 426–431.
[71] C.E. Petrie Aronin, Y.M. Zhao, J.S. Yoon, N.Y. Morgan, T. Prüstel, R.N. Germain, M. Meier-Schellersheim, Migrating myeloid cells sense temporal dynamics of chemoattractant concentrations, Immunity 47 (5) (2017) 862-874.e3.
[72] I. Barkefors, S. Le Jan, L. Jakobsson, E. Hejll, G. Carlson, H. Johansson, J. Jarvius, J.W. Park, N. Li Jeon, J. Kreuger, Endothelial cell migration in stable

gradients of vascular endothelial growth factor A and fibroblast growth factor 2: effects on chemotaxis and chemokinesis, J. Biol. Chem. 283 (20) (2008) 13905–13912.
[73] M. Giacca, S. Zacchigna, VEGF gene therapy: therapeutic angiogenesis in the clinic and beyond, Gene Ther. 19 (6) (2012) 622–629.
[74] P.R. Girard, R.M. Nerem, Shear stress modulates endothelial cell morphology and F-actin organization through the regulation of focal adhesion-associated proteins, J. Cell. Physiol. 163 (1) (1995) 179–193.
[75] M.B. Simmers, A.W. Pryor, B.R. Blackman, Arterial shear stress regulates endothelial cell-directed migration, polarity, and morphology in confluent monolayers, Am. J. Physiol. Heart Circ. Physiol. 293 (3) (2007) H1937–H1946.
[76] L. Lamalice, F.Le Boeuf, J. Huot, Endothelial cell migration during angiogenesis, Circ. Res. 100 (6) (2007) 782–794.
[77] L.P. Diebold, H.J. Gil, P. Gao, C.A. Martinez, S.E. Weinberg, N.S. Chandel, Mitochondrial complex III is necessary for endothelial cell proliferation during angiogenesis, Nat. Metab. 1 (1) (2019) 158–171.
[78] W.H. Oldendorf, M.E. Cornford, W.J. Brown, The large apparent work capability of the blood-brain barrier: a study of the mitochondrial content of capillary endothelial cells in brain and other tissues of the rat, Ann. Neurol. 1 (5) (1977) 409–417.
[79] K.D. Falkenberg, K. Rohlenova, Y. Luo, P. Carmeliet, The metabolic engine of endothelial cells, Nat. Metab. 1 (10) (2019) 937–946.
[80] G. Eelen, P.d. Zeeuw, L. Treps, U. Harjes, B.W. Wong, P. Carmeliet, Endothelial cell metabolism, Physiol. Rev. 98 (1) (2018) 3–58.
[81] F. Gao, T. Mao, Q. Zhang, J. Han, W. Sun, Z. Li, H subtype vascular endothelial cells in human femoral head: an experimental verification, Ann. Palliat. Med. 9 (4) (2020) 1497–1505.